Reg Environ Change
DOI 10.1007/s10113-013-0562-z

ORIGINAL ARTICLE

Multi-GCM projections of future drought and climate variability indicators for the Mediterranean region

Martin Dubrovský · Michael Hayes · Pierpaolo Duce · Miroslav Trnka · Mark Svoboda · Pierpaolo Zara

Received: 7 May 2012 / Accepted: 9 November 2013

Abstract Future climate conditions for the Mediterranean region based on an ensemble of 16 Global Climate Models are expressed and mapped using three approaches, giving special attention to the intermodel uncertainty. (1) The scenarios of mean seasonal temperature and precipitation agree with the projections published previously by other authors. The results show an increase in temperature in all seasons and for all parts of the Mediterranean with good intermodel agreement. Precipitation is projected to decrease in all parts and all seasons (most significantly in summer) except for the northernmost parts in winter. The intermodel agreement for the precipitation changes is lower than for temperature. (2) Changes in drought conditions are represented using the Palmer Drought Severity Index and its intermediate Z-index product. The results indicate a significant decrease in soil moisture in all seasons, with the most significant decrease occurring in summer. The displayed changes exhibit high intermodel agreement. (3) The climate change scenarios are defined in terms of the changes in parameters of the stochastic daily weather generator calibrated with the modeled daily data; the emphasis is put on the parameters, which affect the diurnal and interdiurnal variability in weather series. These scenarios indicate a trend toward more extreme weather in the Mediterranean. Temperature maxima will increase not only because of an overall rise in temperature means, but partly (in some areas) because of increases in temperature variability and daily temperature range. Increased mean daily precipitation sums on wet days occurring in some seasons, and some parts of the Mediterranean may imply higher daily precipitation extremes, and decreased probability of wet day occurrence will imply longer drought spells all across the Mediterranean.

Keywords Mediterranean · Climate change · Global Climate Models · Temperature · Precipitation · Drought · Palmer Drought Severity Index · Weather generator

Electronic supplementary material The online version of this article (doi:10.1007/s10113-013-0562-z) contains supplementary material, which is available to authorized users.

M. Dubrovský (✉)
Institute of Atmospheric Physics, ASCR, 14131 Prague, Czech Republic
e-mail: dub@ufa.cas.cz

M. Dubrovský · M. Trnka
CzechGlobe-Global Change Research Centre, ASCR, 60300 Brno, Czech Republic

M. Hayes · M. Svoboda
National Drought Mitigation Center, School of Natural Resources, University of Nebraska-Lincoln, Lincoln, NE 68583-0988, USA

P. Duce · P. Zara
Institute of Biometeorology, National Research Council, 07100 Sassari, Italy

M. Trnka
Institute for Agrosystems and Bioclimatology, Mendel University, 61300 Brno, Czech Republic

Introduction

The Mediterranean region is considered to be one of the primary climate change hot spots (Giorgi 2006). Alpert et al. (2008) found that the average temperature over the Mediterranean region has increased by 1.5 °C in the last 100 years, and the precipitation across most of this area shows a dominant negative trend in the last 50 years. As a

Published online: 29 November 2013

result of temperature increases accompanied by decreasing precipitation, it is not surprising that many studies have revealed trends toward more frequent and/or more intensive droughts (Brunetti et al. 2002; Piccarreta et al. 2004; Vicente-Serrano et al. 2004). Similar to these observations, the model simulations also indicate that the "transition" toward drier conditions has already started and has accelerated around the turn of the century (Mariotti et al. 2008).

The Global Climate Models (GCM) ensemble projections (IPCC 2007; Mariotti et al. 2008) indicate further increases in temperature and decreases in precipitation in the Mediterranean, which could further exacerbate existing climate-related problems, especially droughts (Mariotti et al. 2008), heat stress (Diffenbaugh et al. 2007) and wildfires (Moriondo et al. 2006). A more detailed projection of future climate in the Mediterranean was made by Giorgi and Lionello (2008), who analyzed outputs from simulations by multiple GCMs from the CMIP3 database and regional climate models (RCMs). Their analysis shows a robust and consistent picture of pronounced climate change over the Mediterranean, which consists of significant increases in temperature (maximum in summer) and decreases in precipitation (especially in the warm season and except for the northern Mediterranean areas in winter). These changes are explained by an increased anticyclonic circulation that yields increasingly stable conditions and is associated with a northward shift of the Atlantic storm track. Giorgi and Lionello (2008) also found that the global and regional model simulations are generally consistent with each other at the broad scale, but the precipitation change signal produced by the regional models shows substantial orographically induced fine-scale structure absent in the global models. In addition, these authors showed that the change signals are robust across forcing scenarios and future time periods, with the magnitude of the signal increasing with the intensity of the forcing. Sanchez et al. (2004) used the regional climate model and focused on the projection of extreme temperature and precipitation events across the entire Mediterranean for the 2070–2100 period and the SRES-A2 emission scenario. They found that (1) daily temperature maxima will increase in general more than daily temperature minima all across the Mediterranean and for all seasons, (2) the daily temperature ranges and extreme temperature values will increase and (3) the extreme precipitation events will significantly change with an increasing trend in many Mediterranean areas, particularly in summer and early autumn. Lionello and Giorgi (2007) analyzed winter precipitation and cyclones as simulated by the regional climate model and concluded that the increases in winter precipitation on the northern Mediterranean coast and the decreases on the southern and eastern Mediterranean coast are due to the increase in the winter cyclone activity over western Europe and its reduction inside the Mediterranean.

This paper follows three aims not seen in previous literature: (1) introducing a new method for mapping the multi-GCM climate scenarios, (2) presenting the future climate scenarios in terms of Palmer Drought Indices and (3) enhancing the future climate scenarios with climate characteristics, which may be derived from daily outputs of GCMs/RCMs and whose inclusion will allow for the diurnal and interdiurnal variability in weather series. First, the changes in seasonal temperature and precipitation are discussed in "Climate change scenarios for precipitation and temperature" section. The mapping method focuses on an explicit inclusion of the quantitative information on the inter-GCM variability into the maps. In addition to the multi-GCM median, the maps show the inter-GCM uncertainty, which allows one to assess the statistical significance of projected changes. The mapping technique is further used in subsequent sections. Second ("Future drought conditions in terms of the Palmer Drought Severity Index" section), the focus is placed on drought, which is one of the hot topics for the entire Mediterranean region (Geeson et al. 2002). The future drought conditions are represented in terms of the Palmer Drought Severity Index (PDSI and its intermediate product, Z-index). The use of this well-established drought index can contribute to a better perception of the future drought risk. Third ("Climate change scenarios in terms of the weather generator parameters"), climate change scenarios, as determined by the change in selected parameters of the stochastic daily weather generator (WG), are given. Inclusion of this approach is motivated by two facts. First, WGs are a well-established tool in disaggregating GCM/RCM-based climate projections into realistic surface weather series required by various climate change impact models. Second, inclusion of the changes in some WG parameters into the climate change scenarios allows to represent changes in diurnal and interdiurnal weather variability, which are of crucial importance for some climate-related processes (e.g., in hydrology and agriculture; Mearns et al. 1996; Dubrovsky et al. 2000, 2004; Moriondo et al. 2011). With the purpose of avoiding misunderstanding, it should be emphasized that the calculation of the changes in WG parameters is the only way of using the WG here.

Data

The present projections are based on the monthly and daily precipitation and temperature outputs from GCM simulations (the database used in IPCC's Fourth Assessment Report—AR4; IPCC 2007). To benefit from the larger signal-to-noise ratio (climate change signal to natural climatic variability), the GCM simulations made with high SRES-A2 emissions were used. The GCMs involved in

Table 1 GCM data used in the analysis. All GCM simulations were made using the SRES-A2 emission scenario from IPCC-AR4

#	Model	Centre	Daily data for use in "Climate change scenarios in terms of the weather generator parameters" section		
			N	Baseline	Future
1	BCM2	Bjerknes Centre for Climate Research, Norway	1	1961–1990	2081–2088
2	CGMR	Canadian Center for Climate Modelling and Analysis, Canada	3	1961–1990	2081–2100
3	CNCM3	Centre National de Recherches Meteorologiques, France	1	1961–1990	2079–2086
4	CSMK3	Commonwealth Scientific and Industrial Research Organisation, Australia	1	1961–1990	2081–2100
5	ECHOG	Met.Inst.Univ Bonn + Met. Res.Inst., Korea + Model and Data Group at MPI-M, Germany			
6	GFCM20	Geophysical Fluid Dynamics Laboratory, USA	1	1961–1990	2081–2100
7	HADCM3	UK Met. Office, UK			
8	HADGEM	UK Met. Office, UK			
9	INCM3	Institute for Numerical Mathematics, Russia			
10	MIMR	National Institute for Environmental Studies, Japan			
11	MPEH5	Max-Planck-Institute for Meteorology, Germany	1	1961–1978	2081–2100
12	MRCGCM	Meteorological Research Institute, Japan			
13	NCCCSM	National Center for Atmospheric Research, USA			
14	NCPCM	National Center for Atmospheric Research, USA			
15	GFCM21	Geophysical Fluid Dynamics Laboratory, USA	1	1961–1990	2081–2088
16	IPCM4	Institute Pierre Simon Laplace, France			

Monthly series used in "Climate change scenarios for precipitation and temperature" and "Future drought conditions in terms of the Palmer Drought Severity Index" sections were available from all listed GCMs (1961–1990 for the baseline climate, and 2070–2099 for the future climate; only 1 realization for each GCM was included). The last three columns specify daily data used in "Climate change scenarios in terms of the weather generator parameters" section (column *N* indicates the number of realizations). Monthly series were downloaded from the IPCC's Data Distribution Centre (http://www.ipcc-data.org/gcm/monthly/SRES_AR4/index.html), and the daily series were extracted from the WCRP database (https://esg.llnl.gov:8443/index.jsp)

each of the three parts of the present analysis are listed in Table 1. The future climate projection relates to the end of the twenty-first century using the 1961–1990 period as a baseline. Note that the database of the daily GCM series used in "Climate change scenarios in terms of the weather generator parameters" section differs from the monthly database used in "Climate change scenarios for precipitation and temperature" and "Future drought conditions in terms of the Palmer Drought Severity Index" sections in two aspects: (1) fewer GCMs are available with a daily database, and (2) while 2070–2099 is used as the future period when working with the monthly database, the shorter period (2081–2100) was used to represent the future in "Climate change scenarios in terms of the weather generator parameters" section because of the limitedness of the daily database. A few GCMs provide longer series, but we preferred to use only time slices made available by most of the GCMs. Even in this case, some GCMs (BCM2, CNCM3, MPEH5) had shorter series, which was accounted for by giving lower weights to these models when deriving the multi-GCM scenarios. In the case of the CNCM3 model, whose daily series output is only available up to 2086, two additional years (2079 and 2080) were added to get the same length as the other two above-named GCMs (the resultant small differences in a future time period may have only a slight effect on the scenarios, and this effect was ignored when processing the data).

To run the PDSI model, the required soil moisture parameter was taken from the global map of texture-based potential storage of water developed by Webb et al. (1993), which is made available at: http://www.ngdc.noaa.gov/ecosys/cdroms/ged_iia/datasets/a12/wr.htm at a $1^\circ \times 1^\circ$ spatial resolution.

Climate change scenarios for precipitation and temperature

Additive changes in temperature (given in °C) and multiplicative changes in precipitation (given in percentages) are derived by comparing average values of temperature and precipitation during the 2070–2099 versus 1961–1990 time slices.

Figures 1 and 2 (Figures SM1 and SM2) show multi-GCM changes in precipitation and temperature for summer and winter (spring, autumn and whole year). The maps were

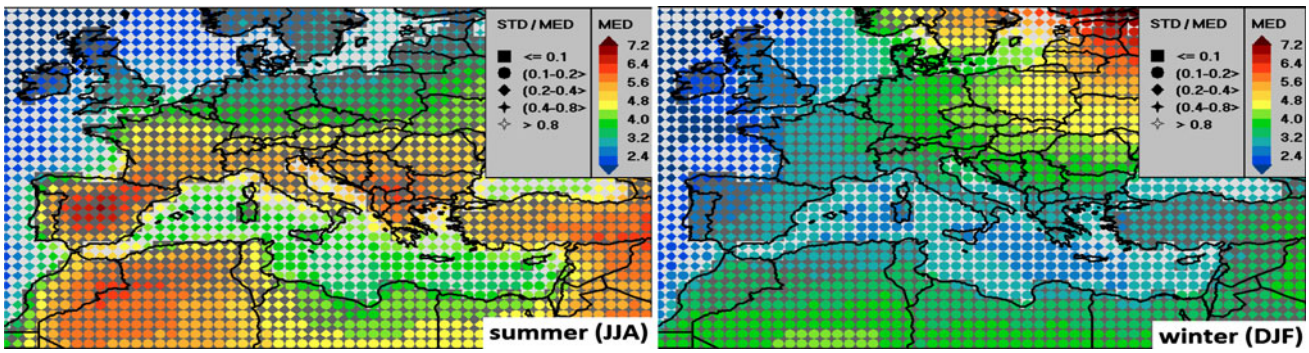

Fig. 1 Multi-GCM changes in summer and winter surface temperature (°C) related to SRES-A2 emission scenario and 2070–2099 (vs. 1961–1990). The *color* represents the median of the values from a set of 16 GCMs; the *shape of the symbol* represents the inter-GCM variability in terms of the STD/MED (standard deviation to median) ratio. See Fig. SM1 for maps related to spring, autumn and annual means of the temperature changes

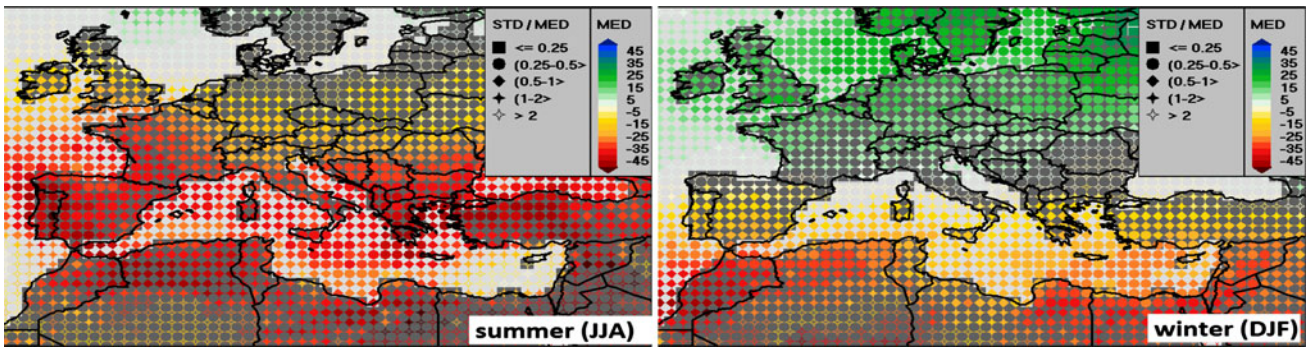

Fig. 2 Multi-GCM changes (%) in summer and winter precipitation sum related to SRES-A2 emission scenario and 2070–2099 (vs. 1961–1990). The *color* represents the median of the values from a set of 16 GCMs; the *shape of the symbol* represents the inter-GCM variability in terms of the STD/MED (standard deviation to median) ratio. See Fig. SM2 for maps related to spring, autumn and annual means of the precipitation changes

created in three steps: (1) GCM-specific scenarios were derived from each of the 16 GCMs for all GCM-specific grids, (2) the scenarios were re-gridded into a common $1^\circ \times 1^\circ$ grid and (3) the medians and standard deviations from the 16 values were calculated for each grid. The maps show a multi-GCM median by the color (the median was used instead of the average to reduce the effect of outliers) together with the inter-GCM uncertainty, which is given in terms of the STD/MED (standard deviation to median) ratio and is shown by the shape of the symbol. Based on the Student test in which the median is used instead of the mean, the change may be considered statistically significant (approximately at the 95 % level) when $|\text{STD/MED}| < 2$. Because the CMIP3-based climate projections have already been discussed in many publications (e.g., IPCC 2007; Giorgi and Lionello 2008), only the main points will be mentioned here, with an emphasis on the inter-GCM variability.

a. *Temperature* is projected to increase in all seasons and for all parts of the Mediterranean. The largest increase occurs in summer, and the smallest increase happens in winter and spring. Considering the spatial pattern, the largest increase is projected for the Balkan and Iberian peninsulas (above 6 °C in their interiors in summer) and the smallest (below 2.8 °C in spring and winter) over the Mediterranean Sea. The inter-GCM agreement is very high in all seasons; the STD/MED is below 0.4 everywhere in all seasons (and below 0.2 in winter and autumn nearly everywhere), which indicates a high statistical significance of the temperature increase.

b. *Precipitation* change is affected by much higher (compared to temperature) inter-GCM variability (note that the symbol scale is different from the one used for the temperature changes in order to adequately display the wider range of the STD/MED values). The maps related to the four seasons reveal the zonally positioned band of high inter-GCM uncertainty (indicating the statistically insignificant multi-GCM changes), which moves toward the south in winter (centered approximately along the 42° N latitude) and toward the north in summer (reaching Scandinavia outside the map). Precipitation is projected to increase north of this band (in the Mediterranean area, this applies only

to its northernmost parts during winter) and decrease south of the band. In winter, the band of high uncertainty (STD/MED > 2) affects major parts of the Mediterranean (minor areas of high uncertainty occur in summer in the eastern Mediterranean). During the other three seasons, the Mediterranean lies mostly south of this band and experiences moderate (spring and autumn) to high (summer) decreases in precipitation. The largest decrease (reaching a 45 % reduction) may be expected in summer across the southern Balkan region (and adjacent Aegean Sea area) and southwest Iberian Peninsula (and adjacent sea area between Spain and Morocco). In terms of the annual change, the Mediterranean area may expect to see a 5–30 % (from north to south) precipitation decrease, and an even higher decrease in its westernmost and easternmost parts.

The above results fit the IPCC projection (Fig. 11.5 in IPCC 2007) well in terms of the spatial patterns and magnitudes of median changes and also in terms of the position of the uncertainty band. The minor differences (including the slightly higher magnitude of changes found in our projection) are due to differences in time slices representing present and future, emission scenario and number of GCMs (IPCC projection was based on 2080–2099 vs. 1980–1999 changes derived from 21 GCM simulations run with SRES A1b emissions).

Future drought conditions in terms of the Palmer Drought Severity Index

Introduction

Drought conditions are commonly expressed in terms of various drought indices [see, e.g., Keyantash and Dracup (2002) and Heim (2002) for reviews]. One of the most commonly used indices is the Palmer Drought Severity Index (PDSI; Palmer 1965). The algorithm has been described previously (e.g., Quiring and Papakryiakou 2003; Wells et al. 2004), so only a brief description will be given here. Based on a supply-and-demand model for the amount of moisture in the soil, PDSI values reflect how the soil moisture at a location compares with normal conditions. A given PDSI value is calculated by using a combination of the current conditions along with previous PDSI values, so that a single PDSI value is not representative of just the current conditions, but also of prior conditions, to a lesser extent. The Z-index is an intermediate product of the PDSI algorithm. It characterizes the immediate monthly water balance anomaly; the PDSI is derived from a series of Z-index values.

The PDSI has been used in many studies (e.g., Byun and Wilhite 1999; Zou et al. 2005), including the larger-scale studies focused on the whole globe (Dai et al. 2004), North America (Karnauskas et al. 2008) and Europe (Lloyd-Hughes and Saunders 2002; van der Schrier et al. 2006). As such, it has become a standard component of drought monitoring efforts (e.g., Svoboda et al. 2002). Dubrovsky et al. (2009) emphasized that the PDSI index is advantageous for assessing the potential impacts of climate change on drought (compared to just precipitation-based indices), as it also accounts for the effect of temperature, which may be a dominant feature, especially in those areas where the precipitation changes are small or insignificant. Only recently Vicente-Serrano et al. (2010) proposed a new SPEI index (Standardized Precipitation Evapotranspiration Index), which is also dependent on precipitation and temperature and could be used to assess drought conditions under global warming.

In this study, both indices were produced by modifying the self-calibrated PDSI code (Wells et al. 2004) available from the National Drought Mitigation Center and the Department of Computer Science and Engineering located at the University of Nebraska-Lincoln. The modification (Dubrovsky et al. 2009), which is analogous to Mavromatis (2010), consists of implementing an option for using two different weather series in a two-step algorithm: in the first step, the PDSI model is calibrated using the reference temperature and precipitation series, and in the second step, it is applied on the test series related to a different period or different site. As a result, the relative PDSI (rPDSI) regime in the test period/site is given in terms of applying the normals from the reference period/site. The rPDSI index was used to assess the impact of the GCM-simulated climate change on drought in the Czech Republic (Dubrovsky et al. 2009).

Because the rPDSI is very persistent, with only small intermonthly fluctuations of its values, the shifts in drought conditions due to future climate change exhibit only an insignificant annual cycle. Therefore, the rPDSI is used here to quantify drought changes related only to the whole year. Drought changes related to individual seasons are expressed in terms of the Z-index, which describes deviation of soil moisture of a given month from the long-term mean without considering antecedent soil moisture conditions. The analogous intermediate product of rPDSI will be denoted as rZ. The original self-calibrated PDSI (and also rPDSI if applied to the weather series identical with the calibration series) classifies values within a range of $<-4, +4>$ in about 96 % of the cases. The values above/below zero indicate wetter/drier conditions compared to the normal conditions. The values below -4 and above $+4$ indicate extreme drought or extreme wet conditions. The range of the Z values is narrower and the $<-2.7, 2.7>$ interval encompasses about 96 % of Z values.

Results and discussion

The change (2070–2099 vs. 1961–1990) in the drought risk is shown in Figs. 3 and SM3 in terms of the annual mean rPDSI and seasonal means of rZ. The maps were created in the same manner as the maps presented in "Climate change scenarios for precipitation and temperature" section. The PDSI model was run for each grid of each GCM, and the 5-year spin-up period was dismissed from the output rPDSI and rZ series (rPDSI starts from zero and takes some time to get to the values that realistically reflect drought conditions), and the means of rPDSI and rZ were derived from the remaining 25 years. These means were re-gridded into a common $1^\circ \times 1^\circ$ grid, and the medians and standard deviations from the 16 values were calculated for each grid.

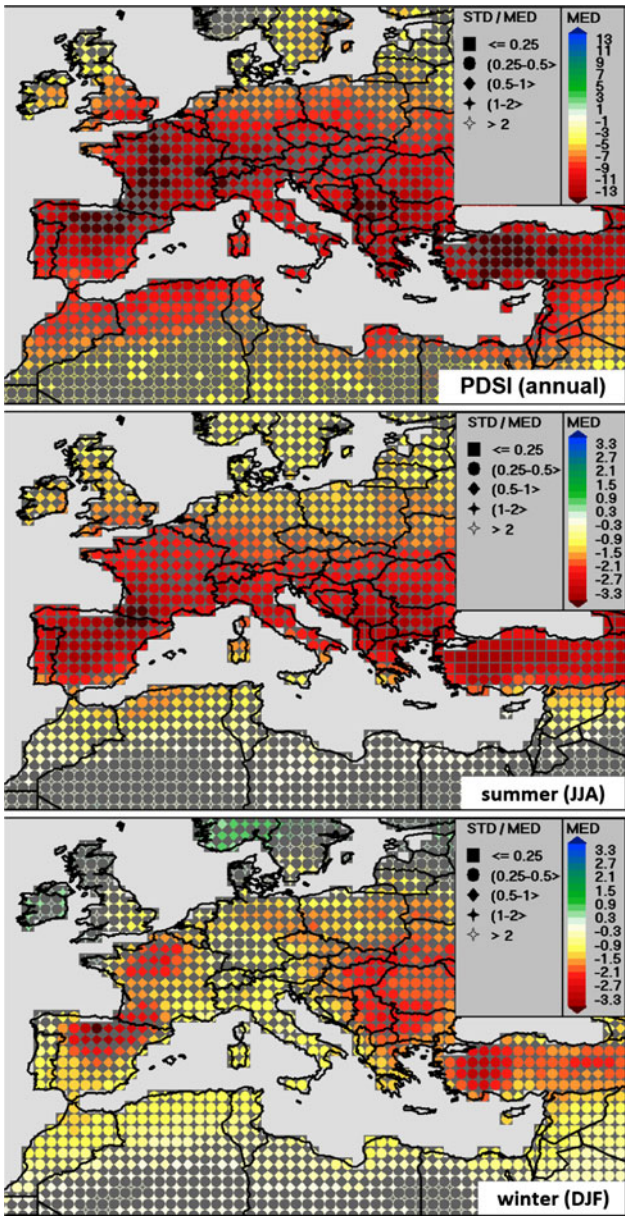

Fig. 3 Annual mean of the relative Palmer Drought Severity Index and seasonal (summer and winter) means of relative Z-index. The indices were calibrated with 1961–1990 and applied to 2070–2099. The multimodel median and STD/MED (standard deviation to median) ratio are represented by *color* and *shape of the symbols*, respectively. See Fig. SM3 for spring and autumn means of relative Z-index

The maps show a significant increase in drought risk, which is a logical consequence of precipitation decreases accompanied by temperature increases. The displayed changes exhibit a high inter-GCM agreement, except for small parts of the North African coast. This may be a consequence of very small precipitation sums in this area with large inter-GCM variability of relative precipitation changes, which leads to a large uncertainty in rPDSI. Figure 3 shows that the mean rPDSI values at the end of the twenty-first century will fall below −4 everywhere (indicating an extreme drought) and even below −8 in many areas, which indicates that the soil moisture levels will be significantly lower than current conditions. These results, which look rather harsh, deserve some comments. First, the present projection relates to the end of twenty-first century and SRES-A2 emission scenario, which is considered among the most extreme emission scenarios. Therefore, the drought conditions for the near future and/or less extreme emissions would be less alarming. Second, the temperature–precipitation conditions in the future target period are significantly different (in terms of both temperature and precipitation) from those during the reference period used to calibrate the PDSI model parameters. From this point of view, the present projection should be considered as the model extrapolation, which is typically affected by larger errors (compared to interpolation). Third, possible overestimation of the magnitude of the rPDSI decrease may be partly due to the fact that the presently used PDSI model calculates potential evapotranspiration using the Thornthwaite algorithm, which is considered less appropriate in warmer climates than the Penman–Monteith formula preferred by recent studies (e.g., Burke et al. 2006; Hoerling et al. 2012; van der Schrier et al. 2013; Dai 2013). To assess the possible effect of using different evapotranspiration formulas, we compared their projections based on the HadCM3 and PDSI (using the Penman–Monteith equation) with projections based on the present PDSI model and the same GCM model (not shown in the figures). The comparison revealed that both model projections are very similar in terms of the spatial pattern, although our magnitude of change is about twice as large as the Burke et al. (2006) results. This allows us to believe that the present multi-GCM projection is comparable to recommended Penman–Monteith-based PDSI if the present magnitudes are accordingly corrected.

Concerning the annual pattern of change in drought conditions, the rZ values show that drought risk will

increase in all seasons, with the most significant increase occurring in summer, which is a consequence of the largest temperature increase accompanied by the largest precipitation decrease. The most significant increase in drought risk is projected to occur in the interiors of the Balkan and Iberian peninsulas and Anatolia, where drought risk will increase significantly in all seasons.

To compare the present results with results by other authors, two studies based on multi-GCM projections will be considered. Because individual studies differ in the drought-related characteristic, set of models and specification of future periods, we give only a rough comparison.

Wang (2005) analyzed winter and summer soil moisture content in the after-stabilization period (2101–2200) in SRES-A1b simulations with 15 GCMs from the CMIP3 database. Our maps of summer and winter means of rZ agree well with Wang's projection [shown in Figs. 3–4 in Wang (2005)] in terms of both the spatial pattern of changes toward higher drought risk and inter-GCM consistency. This fit indicates that the mean GCM-simulated soil moisture is well correlated with the soil moisture simulated by the present PDSI model. Sheffield and Wood (2008) analyzed the occurrence of short-term (4–6 month duration) and long-term (more than 12-month duration) droughts defined as extended periods of anomalous low soil moisture. Their analysis was based on 8 GCMs from CMIP3 and relates to 2070–2099 and 3 SRES emission scenarios (A1b, A2 and B1). In agreement with our PDSI worldwide simulations (Fig. 3 shows only Europe, but simulations were made for whole globe), they found that the Mediterranean is among the regions that show the largest increases in long-term drought occurrence in the future, with the Iberian and Balkan Peninsulas and Anatolia exhibiting the most significant increases.

Climate change scenarios in terms of the weather generator parameters

Introduction

The weather series representing future climate are often produced by WGs (e.g., Wilks 1992; Semenov et al. 2010), whose parameters representing the stochastic structure of the present climate weather series are derived from the observed station-specific weather series and then modified in accordance with the GCM-based (or RCM-based) climate change scenarios. The scenarios commonly include changes in the means of relevant climatic characteristics, but optimally they should also include changes in other characteristics that drive the interdiurnal weather variability. These characteristics, however, cannot be derived from the monthly GCM outputs, but rather from the daily outputs. To address this requirement, the climate change scenarios defined in terms of the WG parameters (hereafter referred to as WG-friendly climate change scenarios) derived from the GCM-simulated daily weather series are included in the present study. The term "WG-friendly" relates to the fact that these scenarios are easily applicable through changes in the WG parameters so that they represent the future climate.

In this analysis, we use M&Rfi, which is the WGEN-like (Richardson 1981) parametric WG and a more flexible follow-on of the Met&Roll (Dubrovsky et al. 2000; Dubrovsky et al. 2004). Both Met&Roll and M&Rfi are being used in current climate change impact studies (e.g., Trnka et al. 2004, 2011; Rötter et al. 2011). Whereas Met&Roll was strictly a daily four-variate WG, M&Rfi may deal with an optional number of variables and optional length of the time step. It also allows the user to apply various transformations of modeled variables and involves other improvements. In the present version, M&Rfi runs with a daily time step and models three variables: daily precipitation amount (PREC), daily average temperature (TAVG) and daily temperature range (defined as the difference between daily temperature extremes; DTR = TMAX − TMIN). Precipitation is a primary variable: wet day occurrences are generated by a Markov chain model (first order is used here), and the precipitation amount is derived from a gamma distribution when a wet day is identified. Standardized values of TAVG and DTR are modeled using a first-order autoregressive model in which their averages and standard deviations are conditioned on the precipitation amount, and the annual cycles are smoothed by a robust locally weighted regression (Solow 1988). The set of WG parameters thus includes two parameters of gamma distribution, two parameters of the first-order Markov chain and "wet day" and "dry day" averages and standard deviations of the non-precipitation variables. More details on this type of the generator, including the results of the validation tests, may be found in Dubrovsky et al. (2000, 2004).

The WG-friendly climate change scenarios are determined by comparing WG parameters calibrated from the GCM slices representing future (2081–2100) versus present (1961–1990) climates, after the trends have been removed (separately for individual time slices). Changes in averages of TAVG are determined by subtracting future minus present values. Changes in precipitation sums, wet day precipitation amounts (being a product of the two gamma distribution parameters), Markov chain model probabilities, daily temperature range and standard deviations of the non-precipitation variables are assumed to be multiplicative and are determined as a ratio of the future versus present climate values. To address the climatic characteristics related to interdiurnal weather variability, the WG parameters listed in Table 2 were included into the

Table 2 List of weather generator parameters included in the present analysis

Acronym	Definition
aTAVG, sTAVG	Average and standard deviation of daily average temperature
aDTR, sDTR	Average and standard deviation of daily temperature range (DTR = TMAX − TMIN)
Pwet	Probability of wet day occurrence (parameter of the first-order Markov chain)
Pdw	Probability of wet day occurrence following the dry day (parameter of the first-order Markov chain)
DPA	Mean daily precipitation amount on a wet day (being a product of the two gamma distribution parameters)

analysis (aTAVG and aDTR were included to complete the picture of the scenario derived from the daily GCM output).

Results

The WG-friendly climate change scenarios derived from GCMs listed in Table 1 were developed for 30 Mediterranean sites (Fig. 4). Similar to the maps in Figs. 1 and 2 and SM1–SM2, the changes in WG parameters presented in Figs. 5, 6, 7 and 8 and SM4–10 are displayed in terms of the multi-GCM median and inter-GCM variability. In contrast to the previous maps, the changes based on individual GCMs were not interpolated. The change related to the closest GCM grid was instead used to determine the GCM-specific changes in individual stations. The reason for doing so is that the interdiurnal variability of surface weather in interpolated GCM-based daily series might be distorted. In discussing the results shown in the maps, we shall focus on the following aspects: (1) magnitude of change, (2) annual cycle, (3) statistical significance of the multi-GCM change (which relates to inter-GCM variability), (4) spatial distribution and (5) potential consequences.

Change in daily average temperature (Δ[aTAVG]; Figure SM4)

The changes in aTAVG mostly correspond to those based on monthly series (Figs. 1 and SM1): they show a maximum increase in summer and a minimum increase in spring

Fig. 4 Location of 30 sites for which the scenarios defined in terms of the weather generator parameters were derived

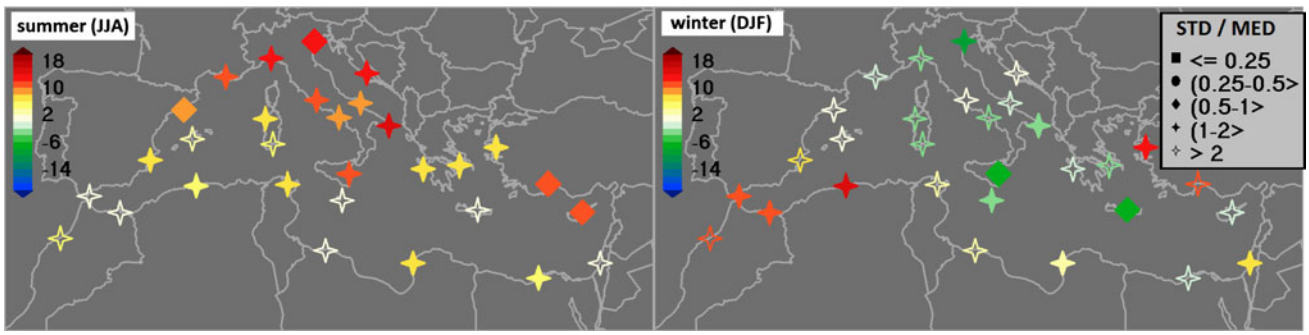

Fig. 5 Summer and winter changes in daily temperature range, Δ(aDTR) [%] (2081–2100 vs. 1961–1990). The *color* represents the median derived from 9 GCM simulations, and the *shape of the symbol* represents the value of the STD/MED (standard deviation to median) ratio. See Fig. SM5 for spring, autumn and annual changes in aDTR

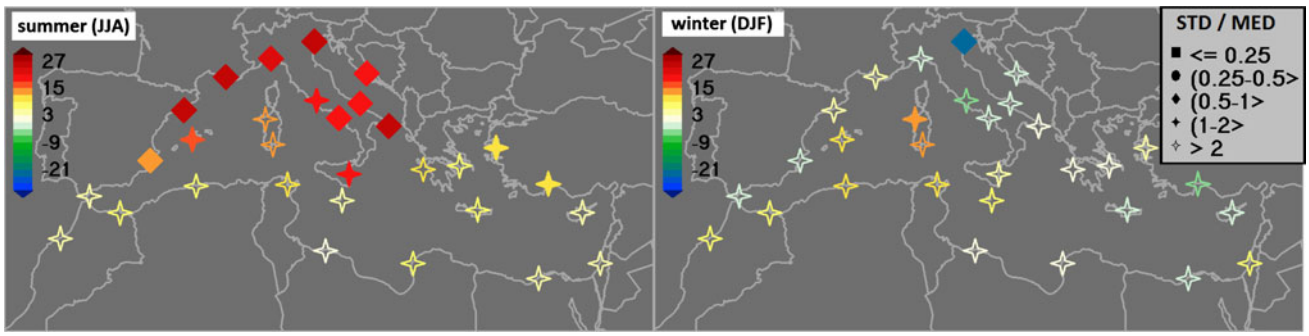

Fig. 6 Summer and winter changes in standard deviation of daily average temperature, Δ(sTAVG) [%] (2081–2100 vs. 1961–1990). The *color* represents the median derived from 9 GCM simulations, and the *shape of the symbol* represents the value of the STD/MED (standard deviation to median) ratio. See Fig. SM6 for spring, autumn and annual changes in sTAVG

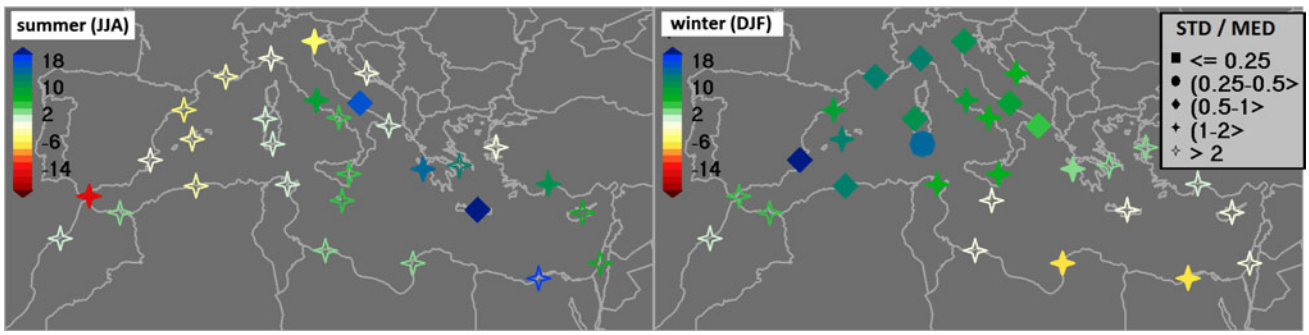

Fig. 7 Summer and winter changes in mean daily precipitation amount on a wet day, Δ(DPA) [%] (2081–2100 vs. 1961–1990). The *color* represents the median derived from 9 GCM simulations, and the *shape of the symbol* represents the value of the STD/MED (standard deviation to median) ratio. See Fig. SM8 for spring, autumn and annual changes in DPA

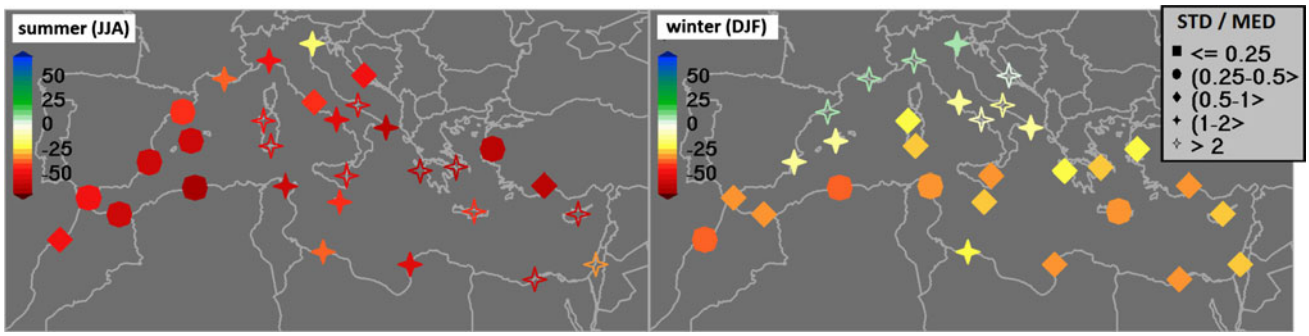

Fig. 8 Summer and winter changes in probability of wet day occurrence, Δ(Pwet) [%] (2081–2100 vs. 1961–1990). The *color* represents the median derived from 9 GCM simulations, and the *shape of the symbol* represents the value of the STD/MED (standard deviation to median) ratio. See Fig. SM9 for spring, autumn and annual changes in Pwet

and winter, along with a high agreement between the GCMs (especially in spring and summer), although the inter-GCM variability in WG-friendly scenarios is somewhat larger (nearly doubled) compared to the scenarios based on monthly GCM data. These differences may be due to the four factors. First, the two databases have different numbers of GCMs. Second, the shorter future time slice in daily datasets (20 vs. 30 year available in the monthly datasets) implies higher uncertainty in determining the changes. Third, the 6-year shift between the centers of the 20- versus 30-year future periods implies a slight bias in projected magnitudes of changes in WG parameters, and this bias relates to a difference of approximately 8 % in greenhouse gas forcing [based on the change in global mean temperature for SRES-A2 scenario extracted from Fig. 10.4 in IPCC (2007)]. Fourth, the statistics for a given individual station shown in Figure SM4 were based on temperature changes related to different geographical locations (being the native grids of individual GCMs), which may somehow increase variability.

Change in daily temperature range (Δ[aDTR]; Figs. 5 and SM5]

The maps show that the changes are mostly positive in all seasons and all locations, except for several locations mostly in the Central Mediterranean in winter and, to a lesser extent, in autumn. The spatial and annual patterns show that the increase should be largest in the north-central Mediterranean in summer and the western Mediterranean in spring and winter. The increase may reach as high as 20 %, which might result in an increase in DTR by 3 °C. Note that the changes are loaded by much higher uncertainty (compared to changes in aTAVG), as indicated by the STD/MED ratio being mostly higher than 1 and often even higher than 2, indicating statistical insignificance of the change in DTR. Seemingly, the change in DTR relates to both TMAX and TMIN. Generally, if DTR increases and aTAVG is unchanged, the avg(TMAX) will increase and avg(TMIN) will correspondingly decrease, which may imply an increased probability of occurrence of temperature extremes.

Change in standard deviations of daily average temperature and daily temperature range (Δ[sTAVG] and Δ[sDTR]; Figs. 6, SM6 and SM7)

Apart from a few cases (including two locations in Turkey), changes in TAVG variability in spring, autumn and winter are mostly statistically insignificant (STD/MED > 2) or only slightly significant ($2 >$ STD/MED > 1). However, even in these seasons (especially in spring and autumn), the maps show good spatial homogeneity, indicated by an increase in sTAVG nearly everywhere in the Mediterranean (locations with possible negative changes are found along the Italian coast). Apparently, the increased temperature variability implies an increased probability of occurrence of extremes. A significant increase in sTAVG in the northern Mediterranean in summer may imply an increased occurrence of extremely high temperatures. Changes in sDTR are affected by even higher uncertainty (compared to sTAVG) and may be considered statistically insignificant except for several locations found primarily in Greece, southern Italy and the northern coast of Africa where a statistically significant decrease in sDTR is projected. The compact cluster of locations in the central Mediterranean with significantly negative changes observed in winter is worth noting. The decrease in sDTR may partly reduce the probability of occurrence of extreme (high or low) temperatures. Not surprisingly, it might be found that the change in sDTR correlates with the change in aDTR: sDTR mostly increases where aDTR increases, which may relate to the fact that the probability distribution function of DTR preserves its shape and changes only in its scale parameter, although this is not a general rule.

Change in the precipitation parameters

Figures 7 and 8 and SM8–SM10 show changes in mean daily precipitation amount on a wet day (DPA parameter), probability of wet day occurrences (Pwet; see Technical Note SM1 in Supplementary Materials for details on determining wet and dry days in GCM outputs) and inter-diurnal variability in precipitation occurrence (Pdw), which all affect changes in short-term precipitation extremes (including the lengths of wet and dry spells). The maps indicate: (1) The decrease in seasonal precipitation sums shown in Figs. 2 and SM2 turns out to be a product of increased DPA (shown in Figs. 7 and SM8) accompanied by a decreased (with a greater magnitude than a DPA increase) Pwet (Figs. 8 and SM9); (2) Changes in Pdw are approximately the same as the Pwet changes, which implies no changes in the persistence of wet/dry day occurrence series (lag-correlation in the first-order Markov chain is expressed as $1 - $ Pdw/Pwet); (3) Lower Pwet (accompanied by the preserved persistence in wet/dry day occurrence series) results in longer dry spells; (4) higher DPA would indicate not just higher daily precipitation means, but higher precipitation extremes would be more likely.

Discussion

Altogether, the WG-friendly scenarios shown in the maps indicate trends toward more extremes in both temperature and precipitation. On the other hand, reasons exist for taking the changes in some WG parameters cautiously. The changes are loaded by higher uncertainty (compared to the scenarios derived from the monthly data) because of a shorter data time period along with greater unreliability of daily time series simulated by the GCMs. The latter fact manifests itself, e.g., by distorted probability distribution functions of daily precipitation. As a result, to get the best use of the changes in those WG parameters, which are affected by larger uncertainty, they should be taken in the proper context, which might include the following: (1) averaging the changes in WG parameters over all GCMs; and/or (2) aggregating information from a set of more neighboring months, e.g., for seasons (instead of producing them strictly based on month-specific scenarios) or using the smoothed annual cycle of month-specific values; and/or (3) applying spatial smoothing.

To compare the present results with results by other authors, the recent study by Sanchez et al. (2004) may serve as a reference. Although their study was based only on a single climate model, whose results may significantly differ from (although without being in contradiction with)

the multimodel ensemble mean, some common features may be found in both studies. Sanchez et al. (2004) found that TMAX will increase in general more than TMIN all across the Mediterranean region and for all of the seasons, which implies increase also in the daily temperature ranges. This finding only partly agrees with the maps in Figs. 5 and SM5, which show rather significant increases in summer (spring) in the northern (western) Mediterranean but trend toward a lower daily temperature range in the central Mediterranean in winter. Increased diurnal temperature variability shown in Figs. 6 and SM6 may be related to higher dispersion of extreme temperature values found by Sanchez et al. (2004). These authors found that the extreme precipitation events will significantly change with an increasing trend in many Mediterranean areas, particularly in summer and early autumn, which partly corresponds to our finding that the mean precipitation amount on rainy days will generally increase (particularly in spring and winter) (Figs. 7 and SM8).

The trend toward longer dry spells implied by the decrease in the probability parameters of the Markov chain model is in qualitative agreement with results of other authors. For example, Beniston et al. (2007) analyzed dry spells (defined as continuous periods of days with no precipitation, commonly referred to as "consecutive dry days," CDD) in the Mediterranean in 2071–2100 based on 3 RCMs and 2 emission scenarios and found that the mean maximum length of CDD in a year will increase over much of the Mediterranean under the SRES-A2 scenario, especially in the southern Iberian Peninsula, the eastern Adriatic seaboard and southern Greece. The impacts are considerably reduced in the SRES-B2 scenario. To get an estimate of the spatial pattern of CDD changes implied by changes in Markov chain model probabilities, we recall that the longest dry spells occur in the dry periods, so that the changes in CDD characteristics may be estimated from changes in Markov chain probabilities related to spring, summer and autumn. Having applied weights 1, 3 and 2 to these three seasons (assuming that dry periods occur mainly from May to October), we may find that the present changes imply the maximum increases in length of dry spells in the western Mediterranean (indicated by the stations located in southeastern Spain and northwest Africa) and southern Greece, which, in fact, corresponds quite well with the results of Beniston et al. (2007). The increase in CDD was also found in a single-GCM study of Sillmann and Roeckner (2007), who made their simulations with ECHAM5/MPI-OM model run with SRES A1b and B1 emission scenarios and found an increase in CDD in nearly all of the Mediterranean (except for the easternmost parts), with the most significant increases in southern parts of the Iberian and Balkan peninsulas and Turkey, which corresponds with results of both Beniston et al. (2007) and our analysis. A similar outcome indicating increasing CDD in the Mediterranean (based on 9 GCMs from the CMIP3 database) was found by Tebaldi et al. (2006).

Conclusions

This paper has presented climate change scenarios for the end of the twenty-first century for the Mediterranean based on a set of SRES-A2 runs of GCMs from the CMIP3 database. Although the CMIP3-based climate projections have already been given a broad discussion in the literature, three aims were formulated at the end of the introductory chapter in order to add some new features to the existing understanding. The results are summarized in the following points; the summary also includes main outcomes of the temperature and precipitation projections, which confirm earlier published results (e.g., IPCC 2007 and Giorgi and Lionello 2008) and provide a basis for the PDSI-based and WG-friendly scenarios presented in "Future drought conditions in terms of the Palmer Drought Severity Index" and "Climate change scenarios in terms of the weather generator parameters" sections.

1. The maps show that all parts of the Mediterranean region may expect increased temperatures in all seasons, with the largest increases occurring in summer and the smallest in winter. In terms of the spatial variability, the largest increases are expected to affect the interiors of the Iberian and Balkan peninsulas, and the smallest increases are projected over the Mediterranean Sea.
2. Precipitation change is affected by much higher (compared to temperature) inter-GCM variability. The zonal band, where the projected precipitation change is not statistically significant, moves southward in winter (being centered approximately along the 42° N latitude) and northward in summer (reaching Scandinavia). Precipitation will increase north of the band and decrease south of the band. The Mediterranean is affected by this band of uncertainty only in winter. The largest reduction in precipitation may be expected in summer nearly everywhere in the Mediterranean, especially in the southern Balkan and Aegean Sea areas. In terms of the annual change, the Mediterranean area may expect a 5–30 % (from north to south) decrease in precipitation.
3. Considering precipitation decreases together with temperature increases, a significant increase in drought risk may be expected in the forthcoming decades. The changes in the drought risk expressed in terms of the Palmer Drought Indices indicate a significant decrease in soil moisture in all seasons, with the most significant decrease occurring in summer. The projections based

on individual GCMs agree in most of the Mediterranean region.

4. The WG-friendly scenarios derived from the GCM daily series provide important additional information on future climate projections, which may be briefly characterized as a trend toward more extreme weather. Temperature maxima will increase not only because of overall change in temperature means, but also because of increases in temperature variability. The decreased total precipitation will be a product of increased daily precipitation sums on wet days accompanied by more significant decreases in wet day probabilities. Importantly, the increased mean daily precipitation sums on wet days occurring in some seasons and some parts of the Mediterranean may imply higher daily precipitation extremes, and the decreased probability of wet day occurrence implies longer drought spells.
5. The WG-friendly scenarios are affected by higher uncertainty because of the shorter time period representing the future along with greater unreliability of daily series simulated by GCMs. Therefore, these scenarios should be used with great care.

Overall, we may conclude that the trends toward the drier and more extreme climate indicated in "Future drought conditions in terms of the Palmer Drought Severity Index" and "Climate change scenarios in terms of the weather generator parameters" sections are in qualitative agreement with projections of other authors (a quantitative agreement was not possible to examine because of different settings of individual experiments). These trends follow the already-started changes, as shown in many studies dealing with the recent trends of drought (see the introduction for the references) and extreme climate indices (e.g., Efthymiadis et al. 2011, Tebaldi et al. 2006).

The WG-friendly climate scenarios presented in "Climate change scenarios in terms of the weather generator parameters" section are freely available (along with the M&Rfi WG) for use in climate change impact studies.

Acknowledgments The paper brings together outputs of the PRASCE project (project IAA300420806 funded by the Grant Agency of Academy of Sciences of the Czech Republic), WG4VALUE project (Project LD12029 funded by Ministry of Education, Youth and Sports) and the National Research Council (Italy)—Academy of Sciences of the Czech Republic bilateral project. The drought index simulations were co-funded by CLIMSAVE 7FP EU project (no. 244031) and the OPVK Project "Building up a multidiciplinary scientific team focused on drought" (No. CZ.1.07/2.3.00/20.0248). Trnka's work was supported by project "Partnership in Climate Research and Adaptation Strategies" (No. CZ.1.07/2.4.00/31.0056) and most recently by Czech-AGRIWAT Project No. LD 13030 funded by Ministry of Education, Youth and Sports. The authors acknowledge the free access to IPCC and WCRP databases derived from the GCM outputs. Last but not least, the authors appreciate comments from two anonymous reviewers who significantly contributed to the final shape of this paper.

References

Alpert P, Krichak SO, Shafir H, Haim D, Osetinsky I (2008) Climatic trends to extremes employing regional modeling and statistical interpretation over the E. Mediterranean. Glob Plan Change 63:163–170

Beniston M, Stephenson DB, Christensen OB, Ferro CAT, Frei C, Goyette S, Halsnaes K, Holt T, Jylhä K, Koffi B, Palutikof J, Schöll R, Semmler T, Woth K (2007) Future extreme events in European climate: an exploration of regional climate model projections. Clim Change 81:71–95

Brunetti M, Maugeri M, Nanni T, Navarra A (2002) Droughts and extreme events in regional daily Italian precipitation series. Int J Climatol 22:509–621

Burke EJ, Brown SJ, Christidis N (2006) Modeling the recent evolution of global drought and projections for the twenty-first century with the Hadley Centre climate model. J Hydrometeor 7:1113–1125

Byun H-R, Wilhite DA (1999) Objective quantification of drought severity and duration. J Clim 12:2747–2756

Dai A (2013) Increasing drought under global warming in observations and models. Nat Clim Change 3:52–58

Dai A, Trenberth KE, Qian T (2004) A global dataset of Palmer Drought Severity Index for 1870–2002: relationship with soil moisture and effects of surface warming. J Hydrometeor 5:1117–1130

Diffenbaugh NS, Pal JS, Giorgi F, Gao X (2007) Heat stress intensification in the Mediterranean climate change hotspot. Geophys Res Lett 34:L11706. doi:10.1029/2007GL030000

Dubrovsky M, Zalud Z, Stastna M (2000) Sensitivity of CERES-Maize yields to statistical structure of daily weather series. Clim Change 46:447–472

Dubrovsky M, Buchtele J, Zalud Z (2004) High-frequency and low-frequency variability in stochastic daily weather generator and its effect on agricultural and hydrologic modelling. Clim Change 63:145–179

Dubrovsky M, Svoboda MD, Trnka M, Hayes MJ, Wilhite DA, Zalud Z, Hlavinka P (2009) Application of relative drought indices in assessing climate change impacts on drought conditions in Czechia. Theor Appl Climatol 96:117–155

Efthymiadis D, Goodess CM, Jones PD (2011) Trends in Mediterranean gridded temperature extremes and large-scale circulation influences. Nat Hazards Earth Syst Sci 11:2199–2214

Geeson NA, Brandt CJ, Thornes JB (Editors) (2002) Mediterranean desertification: a mosaic of processes and responses. J. Wiley & Sons Ltd, Chichester, England, 456 pages, ISBN: 978-0-470-84448-9

Giorgi F (2006) Climate change hot-spots. Geophys Res Lett 33:L08707. doi:10.1029/2006GL025734

Giorgi F, Lionello P (2008) Climate change projections for the Mediterranean Region. Glob Planet Change 63(2–3):90–104

Heim RR (2002) A review of twentieth-century drought indices used in the United States. Bull Amer Meteor Soc 83:1149–1165

Hoerling MP, Eischeid JK, Quan XW, Diaz HF, Webb RS, Dole RM, Easterling DR (2012) Is a transition to semipermanent drought conditions imminent in the U.S. Great Plains? J Clim 25:8380–8386

IPCC (2007) Climate change 2007: The physical science basis. In: Solomon S, Qin D, Manning M, Chen Z, Marquis M, Averyt KB, Tignor M, Miller HL (eds) Contribution of working group I to the fourth assessment report of the Intergovernmental Panel on Climate Change. Cambridge University Press, Cambridge, pp 996

Karnauskas KB, Ruiz-Barradas A, Nigam S, Busalacchi AJ (2008) North American droughts in ERA-40 global and NCEP North American regional reanalyses: a Palmer Drought Severity Index perspective. J Clim 21:2102–2123

Keyantash J, Dracup JA (2002) The quantification of drought: an evaluation of the drought indices. Bull Amer Meteor Soc 83:1167–1180

Lionello P, Giorgi F (2007) Winter precipitation and cyclones in the Mediterranean Region: future climate scenarios in a regional simulation. Adv Geosci 12:153–158

Lloyd-Hughes B, Saunders MA (2002) A drought climatology for Europe. Int J Climatol 22:1571–1592

Mariotti A, Zeng N, Yoon J-H, Artale V, Navarra A, Alpert P, Li LZX (2008) Mediterranean water cycle changes: transition to drier 21st century conditions in observations and CMIP3 simulations. Environ Res Lett 3:044001

Mavromatis T (2010) Use of drought indices in climate change impact assessment studies: an application to Greece. Int J Climatol 30:1336–1348

Mearns LO, Rosenzweig C, Goldberg R (1996) The effect of changes in daily and interannual climatic variability on CERES wheat: a sensitivity study. Clim Change 32:257–292

Moriondo M, Good P, Durao R, Bindi M, Giannakopoulos C, Corte-Real J (2006) Potential impact of climate change on fire risk in the Mediterranean area. Clim Res 31:85–95

Moriondo M, Giannakopoulos C, Bindi M (2011) Climate change impact assessment: the role of climate extremes in crop yield simulation. Clim Change. 104(3–4):679–701

Palmer WC (1965) Meteorological drought. Weather Bureau, Research Paper No. 45, U.S. Department of Commerce, Washington, p 58

Piccarreta M, Capolongo D, Boenzi F (2004) Trend analysis of precipitation and drought in Basilicata from 1923 to 2000 within a Southern Italy context. Int J Climatol 24:907–922

Quiring SM, Papakryiakou TN (2003) An evaluation of agricultural drought indices for the Canadian prairies. Agric Forest Meteorol 118:49–62

Richardson CW (1981) Stochastic simulation of daily precipitation, temperature, and solar radiation. Water Resour Res 17:182–190

Rötter RP, Palosuo T, Virtanen NK, Dubrovsky M, Salo T, Ristolainen A, Fronzek S, Aikasalo R, Trnka M, Carter TR (2011) What would happen to barley production in Finland if global warming exceeded 4 °C? A model-based assessment. Eur J Agron 35:205–214

Sanchez E, Gallardo C, Gaertner MA, Arribas A, Castro M (2004) Future climate extreme events in the Mediterranean simulated by a regional climate model: a first approach. Glob Planet Change 44:163–180

Semenov MA, Donatelli M, Stratonovitch P, Chatzidaki E, Baruth B (2010) ELPIS: a dataset of local-scale daily climate scenarios for Europe. Clim Res 44:3–15

Sheffield J, Wood EF (2008) Projected changes in drought occurrence under future global warming from multi-model, multi-scenario, IPCC AR4 simulations. Clim Dyn 13:79–105

Sillmann J, Roeckner E (2007) Indices for extreme events in projections of anthropogenic climate change. Clim Change 86:83–104

Solow AR (1988) Detecting changes through time in the variance of a long-term hemispheric temperature record: an application of robust locally weighted regression. J Clim 1:290–296

Svoboda MD, LeComte D, Hayes MJ, Heim R, Gleason K, Angel J, Rippey B, Tinker R, Palecki M, Stooksbury D, Miskus D, Stevens D (2002) The drought monitor. Bull Am Meteor Soc 83:1181–1190

Tebaldi C, Hayhoe K, Arblaster JM, Meehl GA (2006) Going to the extremes. Clim Change 79:185–211

Trnka M, Dubrovsky M, Semeradova D, Zalud Z (2004) Projections of uncertainties in climate change scenarios into expected winter wheat yields. Theoret Appl Climatol 77:229–249

Trnka M, Eitzinger J, Semerádova D, Hlavinka P, Balek J, Dubrovský M, Kubu G, Stepanek P, Thaler S, Možny M, Zalud Z (2011) Expected changes in agroclimatic conditions in Central Europe. Clim Change 108:261–289

van der Schrier G, Briffa KR, Jones PD, Osborn TJ (2006) Summer moisture variability across Europe. J Clim 19:2818–2834

van der Schrier G, Barichivich J, Briffa KR, Jones PD (2013) A scPDSI-based global data set of dry and wet spells for 1901–2009. J Geophys Res Atmos 118:4025–4048

Vicente-Serrano SM, González-Hidalgo JC, de Luis M, Raventós J (2004) Drought patterns in the Mediterranean area: the Valencia Region (Eastern Spain). Clim Res 26:5–15

Vicente-Serrano SM, Beguería S, López-Moreno JI (2010) A Multiscalar Drought Index sensitive to global warming: the Standardized Precipitation Evapotranspiration Index. J Clim 23:1696–1718

Wang G (2005) Agricultural drought in a future climate: results from 15 Global Climate Models participating in the IPCC 4th assessment. Clim Dyn 25:739–753

Webb RS, Rosenzweig CE, Levine ER (1993) Specifying land surface characteristics in general circulation models: soil profile data set and derived water-holding capacities. Glob Biogeochem Cycles 7:97–108

Wells N, Goddard S, Hayes MJ (2004) A self-calibrating Palmer Drought Severity Index. J Clim 17:2335–2351

Wilks DS (1992) Adapting stochastic weather generation algorithms for climate change studies. Clim Change 22:67–84

Zou X, Zhai P, Zhang Q (2005) Variations in droughts over China: 1951–2003. Geophys Res Lett 32:L04707